Neuronal mRNAs travel singly into dendrites

Mona Batish[a,b], Patrick van den Bogaard[a], Fred Russell Kramer[a,b], and Sanjay Tyagi[a,1]

[a]Public Health Research Institute and [b]Department of Microbiology and Molecular Genetics, New Jersey Medical School, University of Medicine and Dentistry of New Jersey, Newark, NJ 07103

Edited by Ruth Lehmann, New York University Medical Center, New York, NY, and approved February 6, 2012 (received for review July 12, 2011)

RNA transport granules deliver translationally repressed mRNAs to synaptic sites in dendrites, where synaptic activity promotes their localized translation. Although the identity of many proteins that make up the neuronal granules is known, the stoichiometry of their core component, the mRNA, is poorly understood. By imaging nine different dendritically localized mRNA species with single-molecule sensitivity and subdiffraction-limit resolution in cultured hippocampal neurons, we show that two molecules of the same or different mRNA species do not assemble in common structures. Even mRNA species with a common dendritic localization element, the sequence that is believed to mediate the incorporation of these mRNAs into common complexes, do not colocalize. These results suggest that mRNA molecules traffic to the distal reaches of dendrites singly and independently of others, a model that permits a finer control of mRNA content within a synapse for synaptic plasticity.

long-term potentiation | mRNA localization | RNA granules | single-molecule imaging | synaptic transmission

A number of mRNA species are selectively enriched in neuronal dendrites (1–3). It is believed that they are transported there in a translationally repressed state (4, 5). At synapses that receive sustained stimulation, these mRNAs are locally translated into proteins needed for synaptic differentiation (4–6). This phenomenon is important for the establishment of long-term potentiation and is considered an important cellular correlate of memory (7).

The transport of mRNAs into dendrites is controlled by proteins that bind to RNA motifs called dendritic targeting elements (DTEs), which are often present in the 3′-UTR of these mRNAs (4, 5, 8). The importance of DTEs is underscored by the example of calmodulin-dependent protein kinase IIα (CaMKIIα) mRNA, in which the deletion of the DTE causes the loss of its dendritic localization (9), a drop in the expression of the protein in the dendrites, and an impairment of synaptic plasticity in the organism (10).

It is believed that dendritically localized mRNAs travel as components of ribonucleoprotein complexes (often referred to as RNA transport granules) that serve to keep the mRNA translationally repressed within the soma and during transit (11–13). Distinct from other RNA granules such as stress granules and processing bodies, these granules interface with the cell's active transport mechanisms (14) and carry components of the translational machinery (11, 15). RNA granules contain more than 40 different proteins, some of which are known to bind to the DTEs of transported mRNAs, some of which are part of the translation apparatus, and some of which are associated with the cell's active transport machinery (14, 16). The granules appear to be heterogeneous, as each protein is not found in all of the granules (16).

A number of studies suggest that several different mRNA species can coassemble within the same RNA granule (11, 17–20). Pairs of in vitro-transcribed mRNAs labeled with distinct fluorophores and coinjected into neurons were found to colocalize in common particulate objects (18–20). Endogenous mRNAs encoding CaMKIIα, neurogranin (Nrgn), and activity-regulated cytoskeleton-associated protein (Arc) were found to be colocalized in the same set of granules by fluorescence in situ hybridization (FISH) (18). Also, the fact that individual RNA granules can be imaged with the RNA staining dye SYTO 14 implies that these granules possess a high RNA content (21). Coassembly of more than one mRNA species into the same RNA granule has also been observed in other biological contexts. For example, ASH1 and IST2 mRNAs colocalize in the same structure in the bud tips of yeast (22), and wingless and pair-rule mRNAs travel together to the apical surface of syncytial nuclei in early *Drosophila* embryos (23).

In contrast, a pair of recent studies examined several dendritic mRNAs by FISH and found that some were located in common granules and others were not (20, 24). Another study performed on fibroblasts found that, although the mRNAs encoding arp2, arp3, and β-actin are all concentrated at the leading edges, they do not colocalize with each other (25).

We studied the colocalization of mRNA molecules within neurons, using an imaging technique in which endogenous mRNAs are detected in situ with single-molecule sensitivity (26). Our results demonstrate that the dendritic mRNAs in cultured hippocampal neurons occur singly; i.e., two or more molecules of the same or different mRNA species do not occur together in common complexes.

Results

Different Species of Dendritic mRNAs Are Not Confined in Common Complexes. We obtained single-molecule sensitivity by using ∼50 different hybridization probes, each labeled with a single fluorescent dye, that simultaneously bind to the same mRNA target at different sites within the molecule. Binding of these probes render each mRNA molecule so intensely fluorescent that it can be seen as a bright diffraction-limited spot, whereas background signals from unhybridized probes are of lower intensity and are diffused. Therefore, image processing programs can readily identify and count these spots and are able to determine the location of their centers with great precision (26). Evidence for extremely high specificity and single-molecule sensitivity of this approach and of the accuracy of the spot-detection algorithm is provided in *SI Text* and in Figs. S1 and S2.

We imaged pairwise combinations of eight mRNA species (Arc, β-actin, CaMKIIα, Ef1α, MAP2, Nrgn, PKMζ, and Ube3a) that have all previously been characterized as being dendritically localized (4). One member of each pair was detected with probes labeled with tetramethylrhodamine, and the other member was detected with probes labeled with Alexa 594. For each mRNA species, we observed discrete spots corresponding to individual mRNA molecules. Fig. 1 shows representative results obtained from 4 of the 28 pairwise probe combinations that were studied. Each image is composed of the merged optical slices of an entire cell (*z*-stack). The third panel from left in each pairwise combination represents the color-coded merges of the first two panels. A cursory examination of the merged images indicates that the molecules of the two mRNA species in each pairwise combination do not colocalize with each other.

To explore the degree of colocalization between different mRNA species quantitatively, spots corresponding to the individual molecules of mRNA labeled in each color were

Author contributions: M.B., P.v.d.B., F.R.K., and S.T. designed research; M.B. performed research; M.B. and S.T. analyzed data; and M.B. and S.T. wrote the paper.

The authors declare no conflict of interest.

This article is a PNAS Direct Submission.

[1]To whom correspondence should be addressed. E-mail: tyagisa@umdnj.edu.

This article contains supporting information online at www.pnas.org/lookup/suppl/doi:10.1073/pnas.1111226109/-/DCSupplemental.

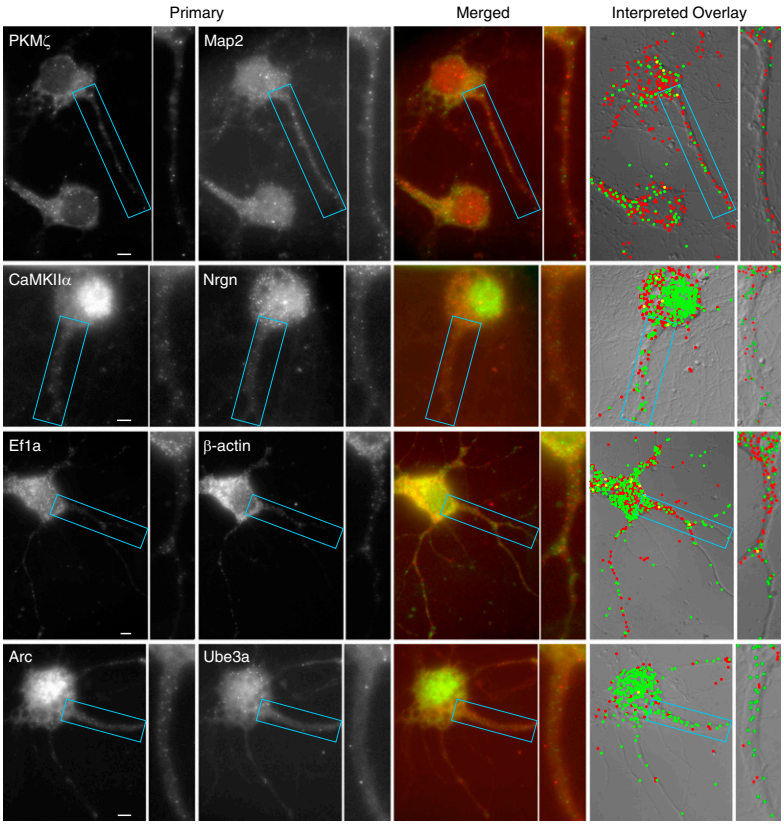

Fig. 1. Individual molecules of different mRNA species do not colocalize with each other. Single-molecule FISH was performed on cultured hippocampal neurons in pairwise combinations of indicated mRNA targets. Gray-scale fluorescence images in the two *Left* column panels are merged images (*z*-stacks) obtained from each fluorescence channel. The color images in the third column were obtained by coding the images in the first column green, the images in the second column red, and then merging them. The *z*-stacks in both channels were analyzed using an algorithm that finds spot-like signals in each image, determines their 3D coordinates, and then looks for spots in one channel that have a counterpart in the other channel that lies within a distance of 250 nm; and if a pair of spots is found to meet that criterion, the algorithm classifies them as being colocalized. The locations of these colocalized molecules (displayed as yellow circles) along with the locations of solitary molecules (displayed as red or green circles) are overlaid onto DIC images of the neurons in the *Right* column panels. Although all 28 pairwise combinations were imaged (Table 1), only 4 of the 28 pairwise combinations are shown here, as these pairs provide representative results for each of the eight mRNAs that were studied. (Scale bars, 5 μm.)

computationally identified, and the 3D coordinates of their centers were determined (Fig. S1). For each spot of a given color, we measured the distances between that spot and all other spots labeled in the other color, thereby determining the distance between that spot and the nearest spot of the other color. The distributions of these "nearest neighbor" distances are presented Fig. S3. If a significant fraction of the two mRNAs in each pair were to be confined within objects as small as an RNA granule, we would have seen a peak corresponding to the size of an RNA granule. Instead, these distributions have means that range from 800 to 1,300 nm. Almost the same distributions are obtained between different molecules of the same mRNA species (Fig. S3 *C* and *D*), indicating that they relate merely to the population density of the mRNAs and to the dimensions and geometry of the neurons. The distributions of sparsely expressed mRNA exhibit longer tails, again suggesting that the distributions relate to the density. These results indicate that the mRNA molecules of two species in a pair do not have a strong tendency to cluster together in objects smaller than the cell size.

Size of RNA Granules. Estimates of the size of neuronal RNA granules range from 100 to 700 nm (11, 15, 16, 21, 27). This uncertainty reflects the variations in the preparation and sources of neurons and homogenates used in different studies. Electron microscopic observations of fractionated homogenates of whole brain and cultured neurons indicate a size range of 100–250 nm (11, 16, 27), whereas a cross-correlation analysis of FISH images in oligodendrocytes suggests a range of 600–700 nm (15). Because the former estimate is more direct, we consider the diameter of RNA granules to be about 250 nm. Because the limit of optical resolution is about the same, a priori, one may expect the spots in two different channels produced by two molecules that are confined within a granule to precisely overlap with each other. However, whereas, on one hand, the centers of diffraction-limited spots can be determined within a few nanometers (28, 29), on the other hand, spectral shifts and other microscopic aberrations may cause the two spots to diverge from each other.

To determine these distances empirically, we imaged each half of the molecules of the same mRNA species (MAP2) with a differently colored set of probes (Fig. 2*A*). The merged raw images in each color (Fig. 2*B*) indicate that most mRNA molecules yield a spot labeled in both colors. The distances from the center of each green spot (corresponding to the left half of MAP2 mRNA) to the center of the nearest red spot (right half of MAP2 mRNA) were determined, and their distributions are shown in Fig. 2*C*. In sharp contrast to the distributions of nearest neighbor distances between two different mRNA species, whose means range from 800 to 1,300 nm, and whose half-maximum heights spread over a range of 1,100–1,900 nm, the distances between the two differently colored spots labeling the same mRNA molecule cluster in a narrow range that centers at 110 nm and spread only as far as 250 nm. An identical distribution was obtained when differently colored probes for mRNA were intermixed by targeting them to alternate sites along the entire length of the mRNA, indicating that the distances measured are not intramolecular distances but instead represent the accuracy of measurement of the same diffraction-limited object in two different channels.

Because, fortuitously, the upper limit of the granule size determined from electron microscopy and the empirical limit obtained above are the same, we classified spots whose centers were less than 250 nm apart as being colocalized. The locations of these colocalized pairs, along with the locations of solitary molecules, are overlaid on differential interference contrast (DIC) images (Fig. 1, *Right* panels). An enlarged image of a pair of spots that are identified as colocalized and another that has closely placed spots, but were considered not to be colocalized by our algorithm, are shown in Fig. S2*C*.

The percentage of colocalization obtained by dividing the number of colocalized mRNAs by the total number of mRNAs in each of the 28 pairwise combinations is presented in Table 1.

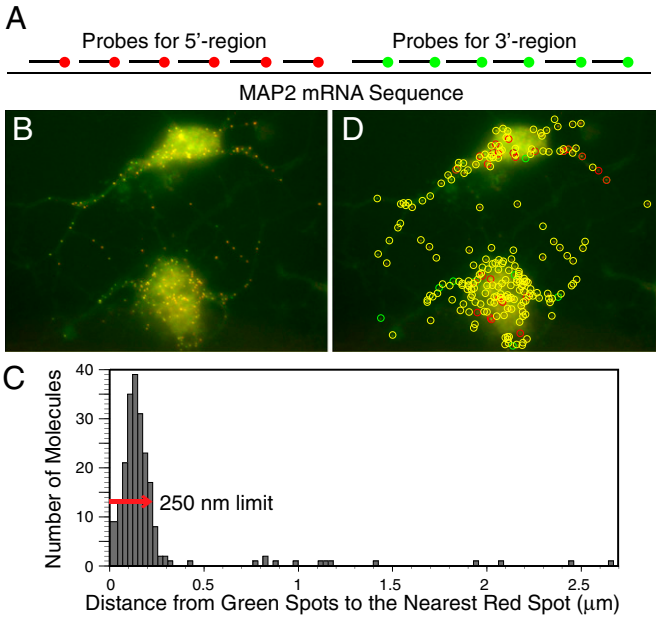

Fig. 2. Determination of empirical distances between centers of spots produced by two probe sets bound to different regions of the same target mRNA. (*A*) Two adjacent regions of MAP2 mRNA were probed with two probe sets labeled with distinct fluorophores. (*B*) Merged raw images of MAP2 mRNA molecules from two fluorescence channels were created while coding the image from one channel with green color and the other with red color. (Scale bar, 5 μm.) (*C*) Distribution of distances from the centers of the green spots to their nearest-neighbor red spots. (*D*) Classification of spots in *B* based on the colocalization distance limit of 250 nm. We found that 73% of all molecules were colocalized, indicating that each probe set may be able to detect 85% of the molecules (*SI Text*).

These low frequencies of colocalization indicate that different mRNAs in the 28 pairwise combinations that were studied have little or no tendency to colocalize. Increasing the limit of colocalization to 300 nm did not change the frequencies of colocalization appreciably. In addition, we present for four pairs of mRNAs, how the frequency of colocalization changes as the colocalization distance is changed continuously up to and beyond the size of the cell in Fig. S3. These distance distributions suggest that the mRNAs have no clear tendency of clustering at any subcellular distance.

Significantly, the frequencies (obtained using the 250-nm limit) were lower in the dendritic compartments than in the bodies of the neurons, where the RNAs are relatively more crowded, indicating that, to the extent that we observe any colocalization, it reflects the likelihood of finding the two molecules in close proximity by chance, rather than due to any specific coassembly into a molecular complex (Tables S1 and S2). Stimulation of neurons by the addition of bicuculline or dihydroxyphenylglycine into the culture medium did not change the frequencies of colocalization appreciably. Similarly, increasing the duration of neuronal culture from 7 to 10 d to 15 to 18 d did not change the frequencies of colocalization substantially.

It can be argued that mRNAs within RNA granules can be so tightly sequestered that they are not accessible to the probes. To address this concern, we imaged one of the mRNAs along with the RNA granule marker protein Staufen 1, which has been shown to associate with the CaMKIIα mRNA (30). Consistent with previous observations, more than 60% of CaMKIIα mRNA molecules were colocalized with Staufen 1 signals, which also appeared as particulate (Fig. S4). Interestingly, the sizes and intensities of the Staufen 1 spots varied much more than the sizes and intensities of the mRNA spots and, consistent with previous studies, other mRNAs did not colocalize with Staufen 1 (30). Furthermore, mRNAs sequestered within the stress granules have been detected using our approach (30), suggesting that mRNA in the granules is accessible to the probes under hybridization conditions.

Dendritic mRNAs Show No Propensity for Self-Oligomerization. To explore whether multiple copies of the same mRNA species are present within RNA granules, we first measured the average number of mRNA molecules per neuron for one of the dendritic mRNA species, MAP2, by FISH and then compared that result to the number of MAP2 molecules per neuron measured by real-time RT-PCR. The number of MAP2 mRNA molecules obtained by the two methods was similar (90 ± 15 molecules per neuron by RT-PCR versus 109 ± 44 molecules per neuron by single-molecule FISH) (Fig. 3). Furthermore, bicuculline stimulation resulted in similar increases in the two measurements (Fig. 3). This analysis was repeated for β-actin mRNA, which resulted in a similar correspondence between the two measurements (Fig. S5). The concordant results obtained by these independent measurements indicate that very few, if any, of the spots that were identified by imaging represent granules possessing multiple copies of the same mRNA.

Any tendency to multimerize would manifest itself in spots of higher fluorescence intensity. If multiple mRNA molecules are confined within an area smaller than the diffraction limit, the apparent fluorescence intensity at that spot should be the sum of the individual intensities of the mRNA molecules present. We measured the maximum intensities within the spots for each dendritically localized mRNA species. The resulting distributions of spot intensities for dendritic populations of MAP2, β-actin, and brain-derived neurotrophic factor (BDNF) mRNAs are shown in Fig. 4. The distributions of intensities of each mRNA species fit well to a unimodal Gaussian distribution (Fig. 4, blue curves). Because the same numbers of singly labeled oligonucleotides (48) were used to image each of these three mRNAs,

Table 1. Percentage of total mRNA molecules that were found colocalized within 250 nm of each other in pairwise combinations

	Arc	MAP2	CaMKIIα	Nrgn	PKMζ	Ube3a	Ef1α
β-Actin	1.80 ± 0.62	2.25 ± 0.33	1.56 ± 0.65	2.46 ± 0.60	1.19 ± 0.39	2.18 ± 0.52	1.60 ± 0.39
Arc		2.09 ± 0.67	3.35 ± 0.82	0.42 ± 0.26	1.13 ± 0.44	0.75 ± 0.53	2.48 ± 0.60
MAP2			3.06 ± 0.54	3.36 ± 0.58	1.82 ± 0.54	3.46 ± 0.97	1.79 ± 0.31
CaMKIIα				1.87 ± 0.56	1.74 ± 0.62	1.97 ± 0.63	2.61 ± 0.86
Nrgn					2.23 ± 0.39	0.33 ± 0.28	0.54 ± 0.16
PKMζ						2.59 ± 0.90	1.37 ± 0.54
Ube3a							0.62 ± 0.21

The percentage of colocalization was calculated by dividing the number of molecules of the lower-abundance mRNA species that were colocalized with the other mRNA species by the total number of mRNA molecules (within a ±95% confidence interval, where at least 10 neurons were examined). The number of spots analyzed ranged from 1,148 to 12,298.

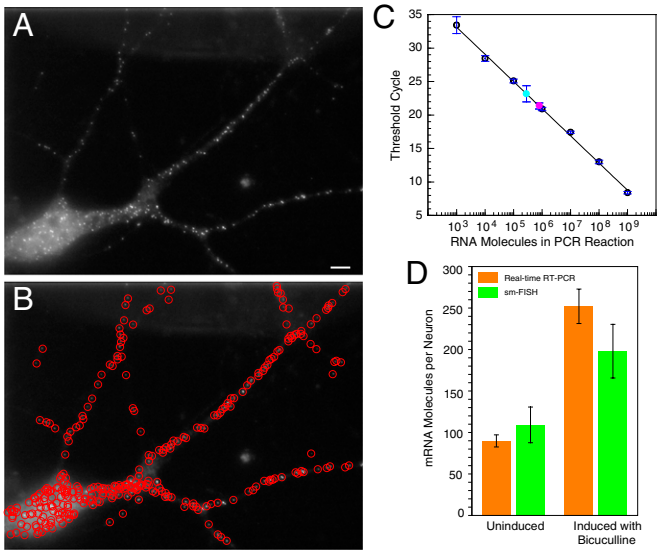

Fig. 3. The number of molecules of MAP2 mRNA per neuron obtained by counting spots in the FISH images is very similar to the number obtained by real-time PCR performed on RNA extracted from the neurons. (*A*) Merged *z*-stacks of neurons imaged after hybridizing with probes for MAP2 mRNA. (Scale bar, 5 μm.) (*B*) Identified spots are overlaid onto the image shown in *A* to demonstrate that almost all MAP2 mRNA molecules are counted by our algorithm. (*C*) Quantification of mRNA copy number by real-time RT-PCR. A standard curve obtained from serial dilutions of full-length in vitro-transcribed MAP2 RNA is shown. The cyan dot identifies the result obtained from a reaction initiated by RNA isolated from resting neurons, and the pink dot identifies the result obtained from a reaction initiated by RNA isolated from the same number of neurons that had been exposed to bicuculline. (*D*) Comparison of the mRNA molecules per neuron determined by single-molecule FISH with the mRNA copy number per neuron determined by real-time PCR. The error bars represent 95% confidence intervals.

the mean intensity of their distributions should be, and were, similar. Furthermore, the mean intensity does not change for a given mRNA species when the number of molecules expressed in the cell is increased substantially by up-regulation (Fig. S2*B*). Although these unimodal Gaussian distributions indicate a priori that most of the granules contain only one "kind" of object, we realized that it was desirable to demonstrate that these optical measurements would indeed be able to identify complexes containing two or more mRNA molecules. We therefore prepared a unique control for each of these three mRNA species.

In the case of MAP2 mRNA (Fig. 4*A*), we prepared a second set of 48 probes labeled with the same fluorophore that bind to a different region of MAP2 mRNA, and we used both sets of probes simultaneously to image native MAP2 mRNAs. Analysis of the resulting images shows that the intensity of the entire population of MAP2 mRNAs is about twice as great as the mean intensity obtained with the first set of probes alone (after subtracting the background intensity from both). To determine the fraction of the spots obtained with the first set of probes alone that are bright enough to be considered as "dimers" and the fraction of spots obtained with both sets of probes simultaneously that are dim enough to be considered as "monomers," we deconvolved the distributions into two different populations (red curves in Fig. 4) with the aid of a "two-component mixed-Gaussian" analysis. In this procedure, the proportions, the means, and the SDs of two Gaussian distributions (five free parameters) are iteratively varied until the two distributions that "best fit" the population distributions are found. The results indicate that "dimers" are a very small fraction (5%) of the spots obtained with the single probe set and that "monomers" are an extremely small fraction (1%) of the spots obtained with the two probe sets combined, indicating that MAP2 mRNA almost always occurs as single molecules in the dendrites.

In the case of β-actin mRNA (Fig. 4*B*), we constructed an artificial gene that contained two tandem copies of β-actin mRNA fused to the coding sequence of GFP. This construct was expressed in the neurons via a lentiviral vector. We probed neurons expressing both the dimeric β-actin mRNA from this construct and the natural β-actin mRNA of the cell, using the same set of 48 probes. Images obtained from these infected neurons showed two kinds of spots: (*i*) spots displaying lower intensity, similar to the intensity of native β-actin mRNA expressed in uninfected cells, and (*ii*) brighter spots due to the presence of the engineered β-actin dimers that were expressed from the lentivirus. The deconvolution of spot intensity distributions indicated that 52% of the mRNA molecules in the infected cells were twice as intense as the natural β-actin. By comparison, the same deconvolution algorithm found that only 2% of the mRNA molecules in the uninfected neurons were twice as intense. Using the intersection of the two Gaussian fit curves as a "cut-off intensity," we classified the spots (Fig. 4*B*, *Right* panels) into low-intensity native β-actin mRNA molecules (red circles) and high-intensity dimeric lentiviral β-actin mRNA molecules (green circles). The infected neurons had many spots of high intensity, whereas the uninfected neurons had only occasional high-intensity spots. Significantly, when the RNAs were also probed with GFP-coding–specific probes, the higher intensity mRNAs were more likely to show colabeling with those probes than mRNAs with unit intensity. These observations indicate that naturally occurring β-actin mRNA is almost always present as a monomer within the neurons.

In the case of BDNF mRNA (Fig. 4*C*), nature provides an appropriate control. BDNF mRNA exits in two isoforms that differ in the length of their 3′-UTR (Fig. S6). Usually about 15–20% of BDNF mRNA has the longer 3′-UTR (31), which is thought to enable this isoform to travel further within a dendrite. We imaged neurons with two sets of probes: one probe set specific for the coding sequence that is common to the two isoforms, and the other probe set specific for the portion of the 3′-UTR that is found only in the second isoform. Both probe sets were labeled with the same fluorophore. We found that 17% of the BDNF mRNA spots in neuronal images displayed a higher intensity than the rest. On the other hand, when only the probe set complementary to the common coding region of the two isoforms was used, only the lower intensity population could be detected. We also imaged BDNF mRNAs with a pair of probe sets that had differently colored fluorophores to distinctly label the longer isoforms. The results of these experiments indicated that 16% of the spots were due to the presence of the longer isoforms (Fig. S6).

These results indicate that BDNF mRNA is also not found as multimers. Indeed, the other six species of dendritic mRNAs that we imaged also displayed unimodal distributions in their intensities, confirming that, in general, dendritic mRNAs do not exist as multimers in neurons (Fig. S7).

mRNAs with a Common DTE Do Not Coassemble into the Same RNA Granules. A rationale proposed for the coassembly of multiple mRNAs into the same transport granule is that transacting proteins bind to common sequence elements present in different mRNAs (17, 20) that are linked together by multivalent scaffolding proteins (17). One such motif, the A2 response element that binds to the heterogeneous nuclear ribonucleoprotein A2, is so short and degenerate that it is found in many mRNAs (18). The dendritic mRNAs CaMKIIα, Nrgn, and Arc contain this sequence element, and it has been reported that more than 70% of these mRNAs are coassembled within common granules (18–20). However, our pairwise colocalization analysis indicates that these mRNAs colocalize with a frequency of 3.35% or less (Table 1 and Table S1). To further explore this issue, we performed FISH simultaneously with three differently colored sets of probes and identified all seven possible combinations of

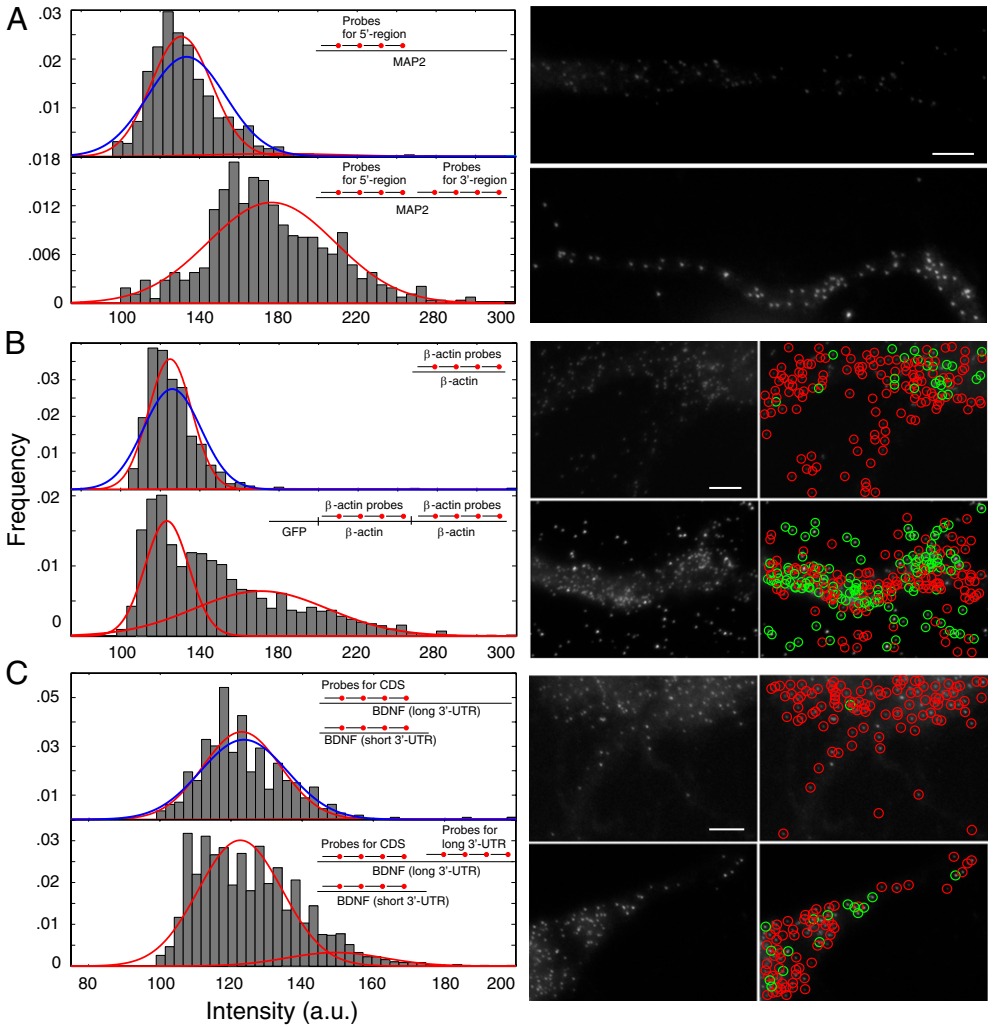

Fig. 4. The maximum intensities of spots produced by three different dendritic mRNAs follow unimodal distributions. (*A*–*C*) *Upper* panels show the data obtained with a single set of 48 probes against native mRNAs, and *Lower* panels are different controls designed to show how the distributions would have looked if the population contained a significant proportion of two or more mRNA molecules within a single granule. To the right of each histogram is a representative image of one of the cells from the population. (*A*) MAP2 mRNA either bound to one set of probes that is specific for one region of each mRNA molecule (*Upper*) or bound to two sets of probes that are each specific for different regions of the same mRNA molecule (*Lower*). (*B*) A set of probes that bind specifically to natural β-actin mRNA was used to image uninfected neurons (*Upper*), and the same set of probes was used to image β-actin mRNA in neurons that had been infected with a lentiviral construct that expresses a tandem dimer of β-actin mRNA that was fused to a sequence encoding GFP (*Lower*). Approximately half of the spots in the images of neurons that contain mRNA molecules possessing the β-actin dimer were twice as intense as the other spots (which arise from endogenous β-actin mRNAs). (*C*) Two different sets of probes were bound to naturally occurring isoforms of BDNF mRNA in neurons. One set of probes bound to a region of the BDNF mRNA that is common to both isoforms, and the other set of probes bound to a region of the BDNF mRNA that occurs only in the longer isoform. Histogram and images resulting from the first set of probes and from both sets of probes. The images to the right of *B* and *C* are overlaid with circles that identify spots of unit intensity (red) and of double intensity (green). The intensities of all of the spots were fitted to a unimodal Gaussian distribution (blue curves) and to a mixture of two Gaussian distributions (red curves). The number of spots analyzed ranged from 446 to 2,306. (Scale bar, 5 μm.)

solitary and colocalized mRNA molecules (Fig. S8*A*). The results of these experiments demonstrate that these mRNAs do not coassemble into common granules. The frequency of colocalization of all three mRNAs within the same granules was found to be less than 1% and is probably an artifact of crowding.

Would longer, well-characterized DTEs mediate coassembly of mRNAs into common granules? The DTEs in several mRNAs have been identified, but none is shared among two or more different mRNA species (4, 20). We therefore created an artificial mRNA encoding GFP and containing the 54-nucleotide-long DTE that occurs in the 3′-UTR of β-actin mRNA (the "β-actin zip code"). Neurons were infected with a lentiviral construct expressing this artificial GFP mRNA, and the mRNA in these cells was then simultaneously hybridized in situ to a probe set that is specific for the coding sequence of β-actin mRNA and to a differently colored probe set that is specific for the coding sequence of GFP mRNA (Fig. S8*B*). The results indicate that, even though both of these mRNAs possess an identical β-actin zip code, and both of these mRNAs migrate to dendrites, they do not coassemble into common RNA transport granules.

Discussion

Several hundred different species of mRNAs have been identified to be in the dendritic compartment in different genome wide screens (1–3). However, the mRNA sets identified in different screens have little overlap with each other. For example, less than 2% of the 260 mRNA species identified in the dendritic compartment by Eberwine et al. (1) were also present in the set of 177 species identified by Poon et al. (2). Therefore, rather then selecting RNAs from these sets, we chose only those that have been individually characterized to be present within dendrites. However, our results suggest that, absent any specific mechanism that brings together mRNAs of a particular pair of species, neuronal mRNAs usually do not cluster together.

How can we reconcile these results with earlier observations in which several different mRNA species were seen to coassemble in common granular structures? The key difference between our method and the methods used in earlier studies is that we use directly labeled probes, which tether the signal to the target. On the other hand, previous methodologies use probes labeled with haptens, which bind to antibodies linked to enzymes that, in turn, convert a small diffusible nonfluorescent substrate (usually tyramide) into a fluorescent precipitate (18, 20). While giving strong fluorescent signals, this technique leads to the spread of the fluorescence signal away from the original location of the target molecule. Consistent with this hypothesis, the spots corresponding to the target mRNA in the previous works appear larger than what we observed and could have led to the incorrect conclusion that mRNAs of different species colocalize with each other. A second line of evidence supporting the coassembly of

multiple mRNA molecules within common granules comes from injection (usually into the cytoplasm) of in vitro-produced and -labeled mixtures of two different mRNA species (18–20). Under these artificial conditions, the amount of mRNA is much greater than what is naturally found in the cell, and the mRNAs are not bound to the retinue of proteins that normally bind to the mRNAs during their synthesis in the nucleus, making aberrant assemblages of mRNAs possible. Furthermore, movement of mRNA molecules in live neurons can cause the dispersal of the fluorescence signals, resulting in an overestimation of colocalization frequency.

Would a larger fraction of mRNAs be found colocalized if a larger limit for colocalization is used? We determined the colocalized fractions for all distances up to the size of neurons (Fig. S3) and found that the number of colocalized molecules increased substantially. However, the distributions of these distances do not show any specific tendency of coassembly into subcellular objects of fixed sizes; instead, these distributions are expected from molecules that are scattered randomly within the confines of neurons.

mRNAs bind to a number of proteins in the nucleus that determine their cytoplasmic fates (32). They are produced at different times at disparate gene loci where they bind cotranscriptionally to their entourage of proteins and are then exported rapidly to the cytoplasm after their release from the chromosome (for most mRNA species, we see only a few molecules in the nucleus at any given moment). Thus, there is little opportunity for them to form multimeric complexes in the nucleus. Furthermore, there is evidence for some mRNAs, such as β-actin mRNA, that transacting proteins that bind to them in the nucleus stay bound to them until they reach their cytoplasmic destination (33). To the extent that these mRNA–protein complexes are remodeled in the cytoplasm of neurons to yield functional RNA transport granules, our results indicate that multiple mRNA molecules are not coassembled within common granules. On the other hand, in the case of *oskar* mRNA in fruit fly oocytes—a system in which mRNAs have clearly been shown to assemble into multimeric complexes—there exists a specific protein that mediates the process of multimerization (34).

The dendritic mRNAs serve diverse, independent, and still poorly understood roles in the process of synaptic differentiation. They are needed at the activated synapses in unique stoichiometries and at unique times. If mRNA granules were composed of multiple mRNAs, we would have to consider highly complex models according to which a granule assembly system in the soma is able to select and package multiple sets of mRNAs into common granules, transport them through dendrites, and then release individual mRNA species from the multiplex granule at the activated synapse (17). The results obtained from our single-molecule imaging studies clarify the picture by suggesting a simpler model in which solitary mRNA molecules bound to their characteristic set of proteins travel to distal reaches of the neurons and respond to the activated synapses individually, providing a finer control to the synapse.

Materials and Methods

We detect mRNA molecules by simultaneously hybridizing about 50 probes to each mRNA species. Hippocampal neurons were cultured on coverslips. After 10 d in culture, they were fixed, permeabilized, and hybridized with probe mixtures. Imaging was performed in oxygen-depleted mounting media. The images were analyzed as described in *SI Materials and Methods*.

The supporting information includes *SI Text*, detailed *SI Materials and Methods*, Tables S1 and S2, Dataset S1, and Figs. S1–S8.

ACKNOWLEDGMENTS. We thank Robert D. Blitzer, Salvatore A. E. Marras, and Gautham Nair. This work was supported by National Institutes of Health Grant MH-079197.

1. Eberwine J, Belt B, Kacharmina JE, Miyashiro K (2002) Analysis of subcellularly localized mRNAs using in situ hybridization, mRNA amplification, and expression profiling. *Neurochem Res* 27:1065–1077.
2. Poon MM, Choi SH, Jamieson CA, Geschwind DH, Martin KC (2006) Identification of process-localized mRNAs from cultured rodent hippocampal neurons. *J Neurosci* 26: 13390–13399.
3. Zhong J, Zhang T, Bloch LM (2006) Dendritic mRNAs encode diversified functionalities in hippocampal pyramidal neurons. *BMC Neurosci*, 10.1186/1471-2202-7-17.
4. Bramham CR, Wells DG (2007) Dendritic mRNA: Transport, translation and function. *Nat Rev Neurosci* 8:776–789.
5. Kindler S, Wang H, Richter D, Tiedge H (2005) RNA transport and local control of translation. *Annu Rev Cell Dev Biol* 21:223–245.
6. Steward O, Worley PF (2001) A cellular mechanism for targeting newly synthesized mRNAs to synaptic sites on dendrites. *Proc Natl Acad Sci USA* 98:7062–7068.
7. Bliss TV, Collingridge GL (1993) A synaptic model of memory: Long-term potentiation in the hippocampus. *Nature* 361:31–39.
8. Martin KC, Ephrussi A (2009) mRNA localization: Gene expression in the spatial dimension. *Cell* 136:719–730.
9. Mayford M, Baranes D, Podsypanina K, Kandel ER (1996) The 3′-untranslated region of CaMKII alpha is a cis-acting signal for the localization and translation of mRNA in dendrites. *Proc Natl Acad Sci USA* 93:13250–13255.
10. Miller S, et al. (2002) Disruption of dendritic translation of CaMKIIalpha impairs stabilization of synaptic plasticity and memory consolidation. *Neuron* 36:507–519.
11. Krichevsky AM, Kosik KS (2001) Neuronal RNA granules: A link between RNA localization and stimulation-dependent translation. *Neuron* 32:683–696.
12. Kiebler MA, Bassell GJ (2006) Neuronal RNA granules: Movers and makers. *Neuron* 51: 685–690.
13. Holt CE, Bullock SL (2009) Subcellular mRNA localization in animal cells and why it matters. *Science* 326:1212–1216.
14. Kanai Y, Dohmae N, Hirokawa N (2004) Kinesin transports RNA: Isolation and characterization of an RNA-transporting granule. *Neuron* 43:513–525.
15. Barbarese E, et al. (1995) Protein translation components are colocalized in granules in oligodendrocytes. *J Cell Sci* 108:2781–2790.
16. Elvira G, et al. (2006) Characterization of an RNA granule from developing brain. *Mol Cell Proteomics* 5:635–651.
17. Carson JH, et al. (2008) Multiplexed RNA trafficking in oligodendrocytes and neurons. *Biochim Biophys Acta* 1779:453–458.
18. Gao Y, Tatavarty V, Korza G, Levin MK, Carson JH (2008) Multiplexed dendritic targeting of alpha calcium calmodulin-dependent protein kinase II, neurogranin, and activity-regulated cytoskeleton-associated protein RNAs by the A2 pathway. *Mol Biol Cell* 19:2311–2327.
19. Mouland AJ, et al. (2001) RNA trafficking signals in human immunodeficiency virus type 1. *Mol Cell Biol* 21:2133–2143.
20. Tübing F, et al. (2010) Dendritically localized transcripts are sorted into distinct ribonucleoprotein particles that display fast directional motility along dendrites of hippocampal neurons. *J Neurosci* 30:4160–4170.
21. Knowles RB, et al. (1996) Translocation of RNA granules in living neurons. *J Neurosci* 16:7812–7820.
22. Lange S, et al. (2008) Simultaneous transport of different localized mRNA species revealed by live-cell imaging. *Traffic* 9:1256–1267.
23. Wilkie GS, Davis I (2001) Drosophila wingless and pair-rule transcripts localize apically by dynein-mediated transport of RNA particles. *Cell* 105:209–219.
24. Mikl M, Vendra G, Kiebler MA (2011) Independent localization of MAP2, CaMKIIα and β-actin RNAs in low copy numbers. *EMBO Rep* 12:1077–1084.
25. Mingle LA, et al. (2005) Localization of all seven messenger RNAs for the actin-polymerization nucleator Arp2/3 complex in the protrusions of fibroblasts. *J Cell Sci* 118: 2425–2433.
26. Raj A, van den Bogaard P, Rifkin SA, van Oudenaarden A, Tyagi S (2008) Imaging individual mRNA molecules using multiple singly labeled probes. *Nat Methods* 5:877–879.
27. Aschrafi A, Cunningham BA, Edelman GM, Vanderklish PW (2005) The fragile X mental retardation protein and group I metabotropic glutamate receptors regulate levels of mRNA granules in brain. *Proc Natl Acad Sci USA* 102:2180–2185.
28. Cheezum MK, Walker WF, Guilford WH (2001) Quantitative comparison of algorithms for tracking single fluorescent particles. *Biophys J* 81:2378–2388.
29. Kubitscheck U, Kückmann O, Kues T, Peters R (2000) Imaging and tracking of single GFP molecules in solution. *Biophys J* 78:2170–2179.
30. Mallardo M, et al. (2003) Isolation and characterization of Staufen-containing ribonucleoprotein particles from rat brain. *Proc Natl Acad Sci USA* 100:2100–2105.
31. An JJ, et al. (2008) Distinct role of long 3′ UTR BDNF mRNA in spine morphology and synaptic plasticity in hippocampal neurons. *Cell* 134:175–187.
32. Trcek T, Singer RH (2010) The cytoplasmic fate of an mRNP is determined cotranscriptionally: Exception or rule? *Genes Dev* 24:1827–1831.
33. Tiruchinapalli DM, et al. (2003) Activity-dependent trafficking and dynamic localization of zipcode binding protein 1 and beta-actin mRNA in dendrites and spines of hippocampal neurons. *J Neurosci* 23:3251–3261.
34. Besse F, López de Quinto S, Marchand V, Trucco A, Ephrussi A (2009) Drosophila PTB promotes formation of high-order RNP particles and represses oskar translation. *Genes Dev* 23:195–207.

Supporting Information

Batish et al. 10.1073/pnas.1111226109

SI Text

Single-Molecule Detection. The principle behind our method is that when all or most of about 50 probes that we use bind to the same mRNA molecule, a spot-like signal is generated, whereas the binding of one or a few probes to nonspecific sites can generate only a diffused signal. Image-processing algorithms designed to detect diffraction-limited spots, and to neglect the diffused signal, can thus be used to locate individual mRNA molecules. This approach was originally introduced more than 10 years ago by Robert Singer and colleagues who used five 50-mer probes, each labeled with multiple fluorophores, for a given mRNA species (1). We modified this method by using about 50, 20-mer oligonucleotides, each labeled with a single fluorophore (2). Our elaboration has proven reliable in yielding single-molecule sensitivity and has successfully been used in a diversity of biological contexts (3–8). The evidence for the high specificity and single-molecule sensitivity that has accumulated thus far is summarized below.

Evidence of High Specificity.

i) Probes against heterologous mRNAs yield spots only when such mRNAs are expressed in the cell. Doxycycline-controlled reporter genes encoding fluorescent proteins and integrated into genomes of various cell lines produce spots only upon removal of doxycycline and not in its presence (2, 6, 8). The same has been shown in the case of mRNA encoding LacZ and luciferase reporters (5, 9). These studies also show that the number of spots observed depends quantitatively on the amount of the inducer used. The same is observed in the case of hippocampal neurons that exhibit spots only when a gene encoding GFP is introduced (Figs. S1*A* and S5*B*).

ii) In the case of inducible natural genes, spots are detected only upon induction, and their numbers correlate with the extent of induction (2, 5). Spots for *STL1* mRNA are seen in yeast upon addition of salt (2), in *c-fos* mRNA in HeLa cells upon addition of serum (8), and in FKBP5 mRNA in lung cells upon addition of a glucocorticoid (2).

iii) In the case of endogenous mRNAs localized in specific subcellular zones, signals were detected only in the appropriate subcellular zones (2, 4, 8). Raj et al. (2) showed that spots corresponding to *elt1* mRNA are seen only in the gut of *Caenorhabditis elegans* embryos; Little et al. (4) showed that *bicoid* mRNA-specific signals are located at the anterior of *Drosophila malenogaster* embryo; and Vargas et al. (8) showed that intron-specific spots are located within nuclei.

iv) Probe-based controls, such as sense (10) or irrelevant probe sets (Figs. S1*A*), do not generate any signals.

v) Finally, signals from two or more distinctly labeled probe sets colocalize when the sets are complementary to the same mRNA, but do not colocalize when the probe sets are complementary to different mRNAs (2, 8) (Fig. 2).

Evidence of Single-Molecule Sensitivity.

i) In the case of three different mRNAs, such as FKBP, GFP, and LacZ mRNA, it has been shown that the number of spots per cell correspond to the number of mRNA molecules per cell obtained by real-time PCR (2, 5, 11).

ii) Deep-sequencing–based mRNA copy number measurements correlate closely to the number of spots that our FISH approach yields. For example, spot counting reveals that neuronal polypyrimidine tract-binding protein is expressed at 25 spots/cell in HeLa cells (8), whereas a deep sequencing study reported 20 copies/cell in NIH 3T3 cells) (12). Similarly, a close correspondence was found between the number of deep sequencing reads and FISH spots for five mRNA species with widely different expression levels in mouse Th2 cells (13).

iii) It has been shown for a number of different mRNA species that, when the same mRNA is probed with two sets of probes, most of the spots colocalize (2, 8) (Fig. 2). In such colabeling experiments performed on MAP2 RNA, we found that about 73% of the molecules are detectably labeled with two probe sets. This colabeling efficiency would be obtained if each probe set is able to detect 85% (square root of 0.73) of the molecules. In the case that a few of the molecules are fragmented due to RNA decay, the detection efficiency will be even higher.

iv) When pre-mRNAs are imaged with two distinctly labeled sets of probes, one for an intron and the other for a coding sequence, the colocalized signal corresponding to pre-mRNAs is restricted to the nucleus, and the number of colocalized spots decrease as splicing progresses (8).

v) Certain mRNAs have two isoforms that differ as to the inclusion of two alternative exons in the mature mRNA. When two distinctly labeled probe sets specific to the alternative exons are hybridized at the same time, the spots generally do not colocalize, except at or near the gene locus where pre-mRNAs that include both exons are present (10).

vi) In the case of two BDNF mRNA isoforms that differ in the length of 3′-UTR, we designed two distinctly labeled probe sets—one against a common region and the other against the longer 3′-UTR. We found that 16% of the spots were colocalized, a frequency that closely resembles the one determined by bulk measurements (14) (Fig. S6).

vii) The magnitude of the intensities scale with the number of probes used (2, 11) and the intensity of the spots is the sum of the intensities of all dye molecules that are tethered to the mRNA molecules (1).

SI Materials and Methods

Neurons. Embryonic hippocampal tissue from embryonic day 18 rats was purchased from Brain Bits. The quality of neurons obtained from this tissue was similar to the neurons obtained from in-house dissection. After triturating the tissue, the cells were plated onto glass coverslips coated with poly-D-lysine and laminin and incubated in Neurobasal Medium supplemented with B27 and glutamine (Invitrogen). The neurons were allowed to grow at 37 °C in an atmosphere containing 5% CO_2 for at least 10 d with medium replenishment occurring every 3 d. For imaging activity-regulated cytoskeleton-associated protein mRNA, we stimulated neurons by the addition of bicuculline (40 μM) or enhanced its expression by the addition of cyclohexamide (50 μg/mL final concentration) that suppresses nonsense-mediated decay that otherwise keeps the levels of this mRNA very low.

Lentiviral Constructs. A DNA fragment corresponding to the full-length rat β-actin gene (NCBI accession no. NM_031144) was amplified from a cDNA clone (MGC:72783; Thermo Scientific). The transfer vector pCS-CG and the packaging plasmids pMD2.G and pSPAX2 for lentivirus production were obtained from Addgene. Plasmid pCS-CG was linearized at its unique BsrGI restriction endonuclease site, and two tandemly arranged copies

of the β-actin fragment were inserted, using the In-Fusion cloning system (Clontech). Cloning resulted in a plasmid containing the tandem β-actin fragments fused in frame with a preexisting GFP-coding sequence. Similarly, a 64-nucleotide-long sequence corresponding to the entire 3′-UTR of β-actin that includes the zip code sequence (15) was placed at the 3′-end of the GFP sequence. Lentiviruses were then generated from the engineered pCS-CG constructs with the aid of helper plasmids (16).

Probe Sets and in Situ Hybridization. Sets of probes that contain 48 labeled oligonucleotides were designed to hybridize to each mRNA target molecule or to a portion of an mRNA target molecule. The sequences of these probe sets (along with the accession numbers of their mRNA target sequences) are listed in Dataset S1. Each set of 48 oligonucleotides was purchased from Biosearch Technologies with a 3′-amino modification, pooled in equimolar amounts, and then coupled to TMR, Alexa 594, or Cy5, using their succinimidyl esters (17, 18). The dye-coupled fractions of the pooled oligonucleotides were purified en masse by HPLC, as described previously (17, 18).

Coverslips containing the neurons were washed with PBS, fixed in PBS containing 3.7% (vol/vol) formaldehyde for 10 min, washed with PBS, incubated with 70% (vol/vol) alcohol for 1 h, washed with 10% formamide dissolved in 2× SSC (Ambion), and then hybridized to one or more probe sets. The hybridizations were performed overnight in a moist chamber maintained at 37 °C, with the coverslips placed upside down over a hybridization solution that was placed on a sheet of Parafilm. Each 50-μL in situ hybridization reaction contained 10% (wt/vol) dextran sulfate (Sigma), 1 μg/μL *Escherichia coli* tRNA (Sigma), 2 mM ribonucleoside-vanadyl complex (New England Biolabs) to inhibit ribonucleases, 0.02% (wt/vol) RNase-free BSA (Ambion), 10% (vol/vol) formamide (Ambion), and 1 ng/μL of each probe set. After hybridization, the coverslips were washed twice in a solution containing 10% formamide and 2× SSC and then mounted in an oxygen-depleted mounting medium (17, 18).

Staufen 1 protein was imaged using an anti-Staufen 1 antibody obtained from Millipore.

Estimation of mRNA Copy Numbers by Spot Counts and by Real-time RT-PCR. Neurons were plated on 24 coverslips (diameter 12 mm) in a common dish. After 8 d of culture, they were segregated into two groups of 12 coverslips each, one of which was treated with bicuculline. After induction, we isolated RNA from nine coverslips in each group using TRIzol reagent (Invitrogen) and fixed the rest of the coverslips. We imaged two of the coverslips in each group using DIC with a 10× objective and counted the total number of neurons (their bodies) in 50 randomly selected fields. We found 42.9 ± 7.0 neurons/field. The area of each field was 0.567 mm^2. Because the area of each coverslip was 113.4 mm^2, there were 199.4 fields in each coverslip. This meant that there were about 8,765 neurons on each coverslip. Because nine such coverslips were the source of the mRNA, we estimated that about 78,886 ± 12,621 neurons contributed to the total RNA. A total of 1/25th of this RNA was introduced into the final reaction (equivalent to RNA from 3,155 neurons).

For real-time RT-PCR, we prepared full-length MAP2 and β-actin mRNA by in vitro transcription using corresponding plasmids as templates. The RNAs were purified using Zymo RNA purification kits (Zymo Research) and quantified using a Nanodrop spectrophotometer (Thermo Scientific). These RNAs were serially diluted and used to create a set of standard curves for the quantification of their corresponding neuronal mRNAs. The RT-PCR was performed in triplicate using a OneStep RT-PCR kit (Qiagen) with SYBR green as indicator. The procedure was repeated again on a different day. The primers used were MAP2 (CTGTGAGTGCAGATGCTGAG and CACAGTACCCCATGTCTTCA) and β-actin (CCAACTGGGACGATATGGAG and AACACAGCCTGGATGGCTAC). The standard curves thus obtained were used to determine the number of molecules in the sample RNA extracted from the neurons.

The remaining coverslips were fixed and used to perform in situ hybridization, imaging, and spot counting with respect to MAP2 and β-actin mRNA. The number of spots from at least 30 sparsely dispersed neurons were counted.

Imaging. An Axiovert 200M inverted, wide-field, fluorescence microscope (Zeiss), equipped with a 1.3 numerical aperture, 100× oil immersion objective, a CoolSNAP HQ camera (Photometrics) cooled to −30 °C, and OPENLAB acquisition software (Perkin-Elmer) were used to acquire the images.

Detection of Spots in Images and Colocalization Analysis. For mRNA counting and colocalization studies, 16–20 *z*-sections separated from each other by 0.2 μm were acquired with 1- or 2-s exposures in each fluorescence channel. The stacks of digital images for each channel were analyzed by a custom program written in Matlab (MathWorks). The program first enhances the particulate signals by filtering the image stacks with a 3D 9 × 9 × 9 Laplacian filter (19). The user then picks a region of interest from the image for which a 3D surface area plot is generated. On the basis of this plot, the user selects a threshold that is just above the noise but well below the signal. Because the signal-to-noise ratios (mean signal intensity divided by the SD of the background level) are usually high (>50), the number of spots that the algorithm picks is robust and relatively insensitive to the choice of threshold (Fig. S1*C*). This threshold is then used to create stacks of binary images in which the spots become 1 and the background becomes 0. The 3D coordinates of the geometric centers of the spots (centroids) are then determined from the binary stacks corresponding to each channel. The distances from each centroid in one channel to the closest centroid in the other channel are then computed. The user-provided distance limit (250 nm in most cases) is then used to classify the spots as colocalized or not. The program is also able to draw circles to produce overlays with raw images and count the number of spots in user-defined regions. The algorithm performs accurately for well-separated spots but misses some spots in crowded regions. The script of the program is available upon request.

Analysis of Intensity Distributions. We determined the intensity of the most intense pixel within the image volume that corresponds to a spot. Although image stacks filtered with the Laplacian filter were used to identify the volume corresponding to the spots, the raw images were used to find the intensity of the most-intense pixel within the spot. The most-intense pixel in this method may not always coincide with the centroid. The intensities of spots from several image stacks were pooled for a given mRNA species and probe set (440–2,400 spots). The intensities of the population of spots were fitted to a simple- and a two-component Gaussian model using the expectation maximization algorithm (20). During the fitting of the two-component Gaussian model, we varied the mean and the SD of each Gaussian and their relative proportions (a total of five free parameters). Before using this algorithm to deconvolve our experimental populations, we tested its efficacy on simulated data that were created from two Gaussians with different mixing ratios, means, SDs, and noise levels.

1. Femino AM, Fay FS, Fogarty K, Singer RH (1998) Visualization of single RNA transcripts in situ. *Science* 280:585–590.

2. Raj A, van den Bogaard P, Rifkin SA, van Oudenaarden A, Tyagi S (2008) Imaging individual mRNA molecules using multiple singly labeled probes. *Nat Methods* 5:877–879.

3. Raj A, Rifkin SA, Andersen E, van Oudenaarden A (2010) Variability in gene expression underlies incomplete penetrance. *Nature* 463:913–918.
4. Little SC, Tkačik G, Kneeland TB, Wieschaus EF, Gregor T (2011) The formation of the Bicoid morphogen gradient requires protein movement from anteriorly localized mRNA. *PLoS Biol* 9:e1000596.
5. So LH, et al. (2011) General properties of transcriptional time series in Escherichia coli. *Nat Genet* 43:554–560.
6. To TL, Maheshri N (2010) Noise can induce bimodality in positive transcriptional feedback loops without bistability. *Science* 327:1142–1145.
7. Topalidou I, van Oudenaarden A, Chalfie M (2011) Caenorhabditis elegans aristaless/Arx gene alr-1 restricts variable gene expression. *Proc Natl Acad Sci USA* 108:4063–4068.
8. Vargas DY, et al. (2011) Single-molecule imaging of transcriptionally coupled and uncoupled splicing. *Cell* 147:1054–1065.
9. Shih JD, Waks Z, Kedersha N, Silver PA (2011) Visualization of single mRNAs reveals temporal association of proteins with microRNA-regulated mRNA. *Nucleic Acids Res* 39: 7740–7749.
10. Waks Z, Klein AM, Silver PA (2011) Cell-to-cell variability of alternative RNA splicing. *Mol Syst Biol* 7:506.
11. Vargas DY, Raj A, Marras SA, Kramer FR, Tyagi S (2005) Mechanism of mRNA transport in the nucleus. *Proc Natl Acad Sci USA* 102:17008–17013.
12. Schwanhäusser B, et al. (2011) Global quantification of mammalian gene expression control. *Nature* 473:337–342.
13. Hebenstreit D, et al. (2011) RNA sequencing reveals two major classes of gene expression levels in metazoan cells. *Mol Syst Biol* 7:497.
14. An JJ, et al. (2008) Distinct role of long 3′ UTR BDNF mRNA in spine morphology and synaptic plasticity in hippocampal neurons. *Cell* 134:175–187.
15. Ross AF, Oleynikov Y, Kislauskis EH, Taneja KL, Singer RH (1997) Characterization of a beta-actin mRNA zipcode-binding protein. *Mol Cell Biol* 17:2158–2165.
16. Tiscornia G, Singer O, Verma IM (2006) Production and purification of lentiviral vectors. *Nat Protoc* 1:241–245.
17. Raj A, Tyagi S (2010) Detection of individual endogenous RNA transcripts in situ using multiple singly labeled probes. *Methods Enzymol* 472:365–386.
18. Batish M, Raj A, Tyagi S (2011) Single molecule imaging of RNA in situ. *Methods Mol Biol* 714:3–13.
19. Gonzalez RC, Woods RE, Eddins SL (2004) *Digital Image Processing Using Matlab* (Pearson Prentice Hall, Upper Saddle River, NJ).
20. Do CB, Batzoglou S (2008) What is the expectation maximization algorithm? *Nat Biotechnol* 26:897–899.

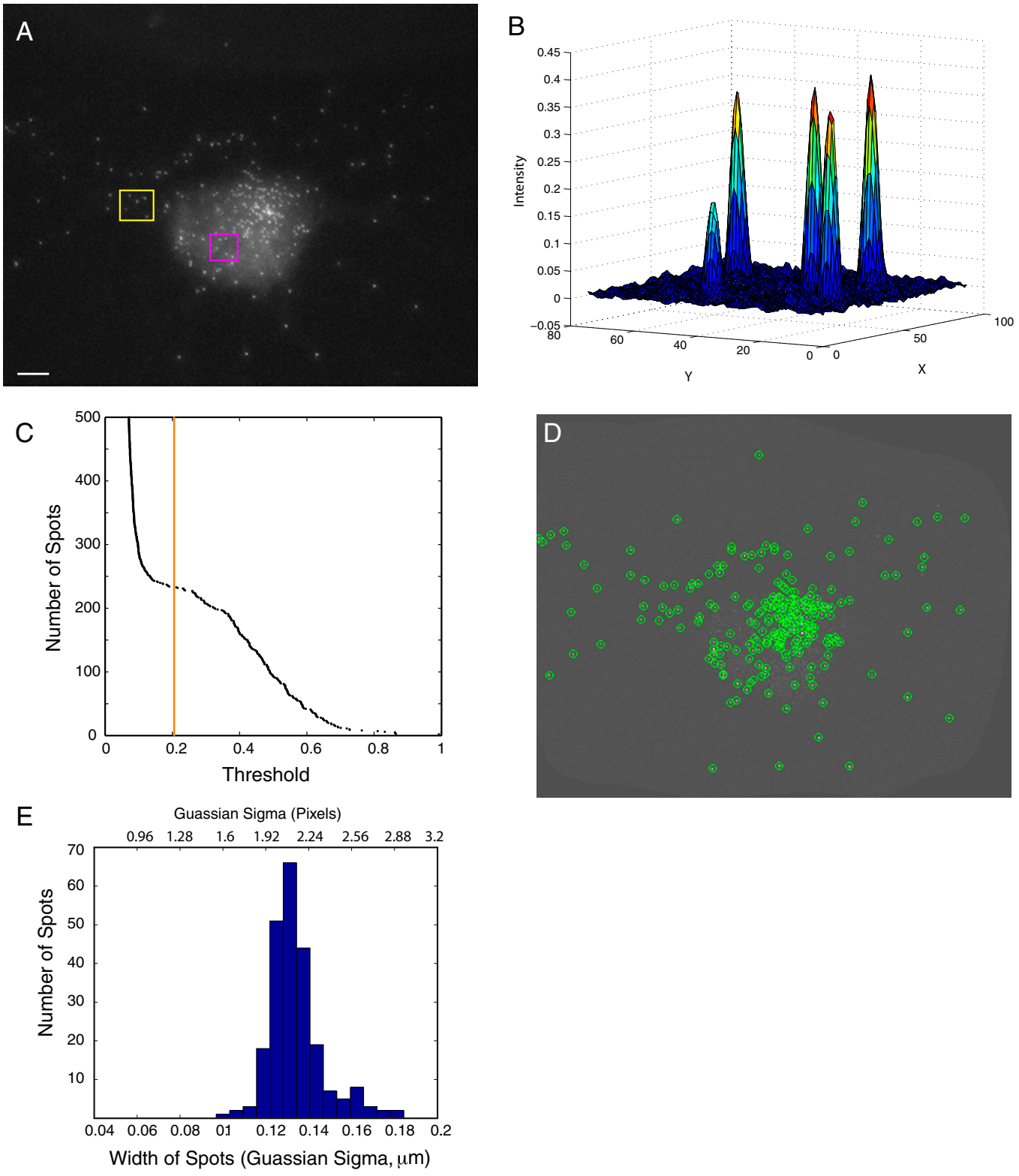

Fig. S1. The basic characteristics of in situ hybridization images and the efficacy of the spot-detection algorithm. (*A*) A merged stack of raw images contrasted to show the spots obtained for MAP2 mRNA. In the region enclosed by the yellow box, the average signal for the five spots was 143.63 ± 10.77; the background level was 98.69 ± 1.14; and the signal-to-noise ratio (signal divided by the SD of the background) was 126.24 ± 10.8. In the region enclosed by the pink box, the average signal for the five spots was 169.34 ± 13.39; the background level was 124.86 ± 2.47; and the signal-to-noise ratio was 53.40 ± 13.62. Usually the signal-to-noise ratios are >50 in our images. (*B*) A surface plot for the area enclosed by the yellow box in *A* after filtering the image with the Laplacian filter. The minimum and maximum intensities in the stack were used to set the intensity scale. (*C*) Relationship between the threshold used to segment the image and the number of spots detected. (*D*) The particles identified by using the threshold shown by the orange line in *C*. (*E*) Width of the spots that were detected in the stack. A 2D Gaussian function was fitted to each spot and the SDs are provided as a measure of the width of the spots. This fitting allows an intensity-independent measurement of the width of the spots. (Scale bar, 5 μm.)

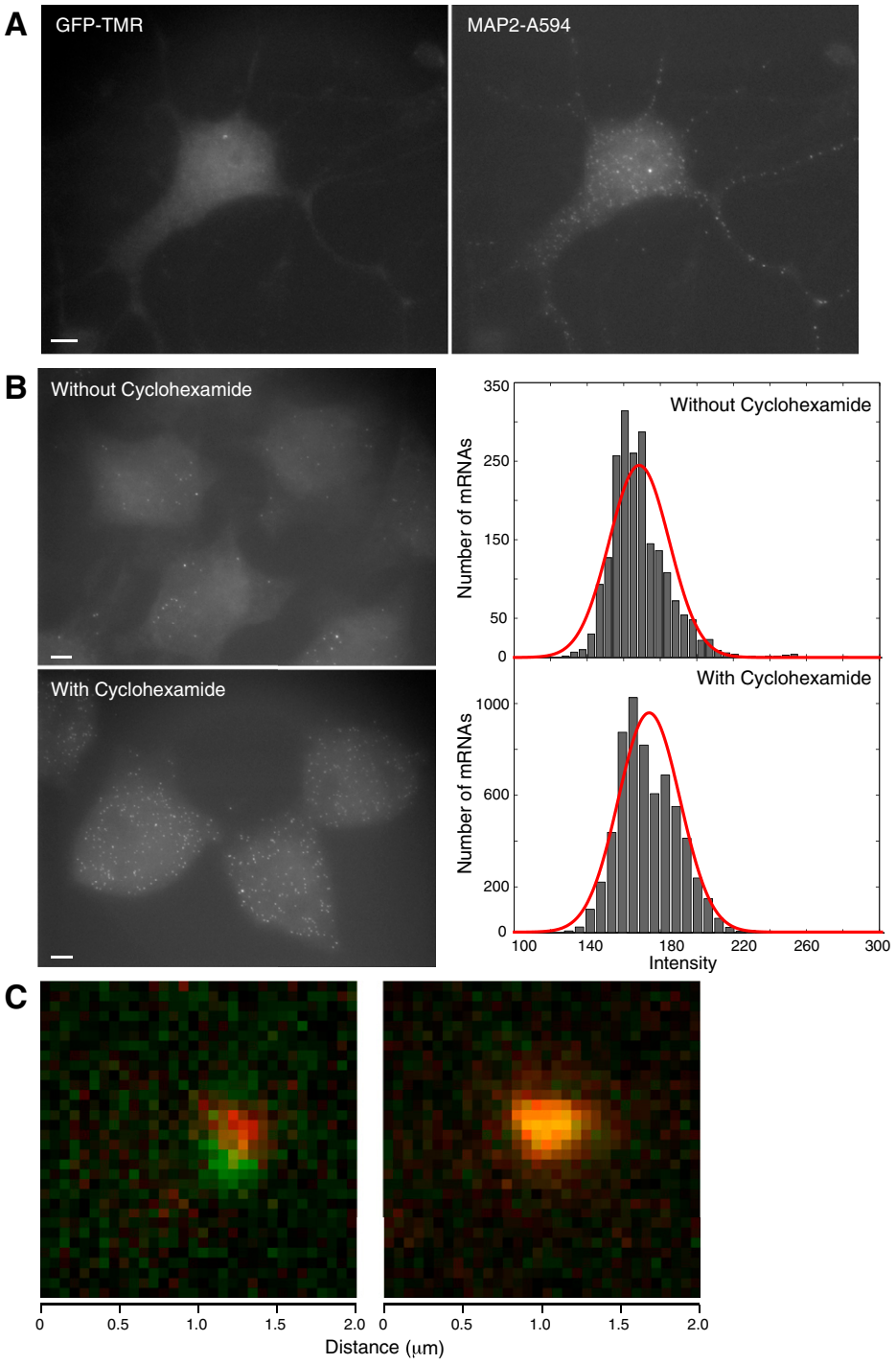

Fig. S2. (*A*) A demonstration of the specificity of the probe sets. A probe set specific to a heterologous RNA (GFP mRNA) that is not expressed in the neurons does not yield any spots, whereas a probe set labeled with another color for an endogenous mRNA (MAP2 mRNA) and included in the same hybridization mixture yields spots. (*B*) The intensity of spots produced by individual mRNA molecules remains the same even when the expression level of the RNA increases threefold. Neuronal polypyrimidine tract binding protein (nPTB) mRNA was up-regulated in HeLa cells by the addition of cyclohexamide that inhibits the nonsense-mediated decay responsible for keeping the nPTB mRNA levels low. (*C*) Enlarged images of a pair of spots that are identified as not colocalized (*Left*) and as colocalized (*Right*) by our algorithm. The first image is from Fig. 1, color merge in the second horizontal panel, and the second image is from Fig. 2 *Left*. Each pixel corresponds to 1/16th of 1 μm. (Scale bar, 5 μm.)

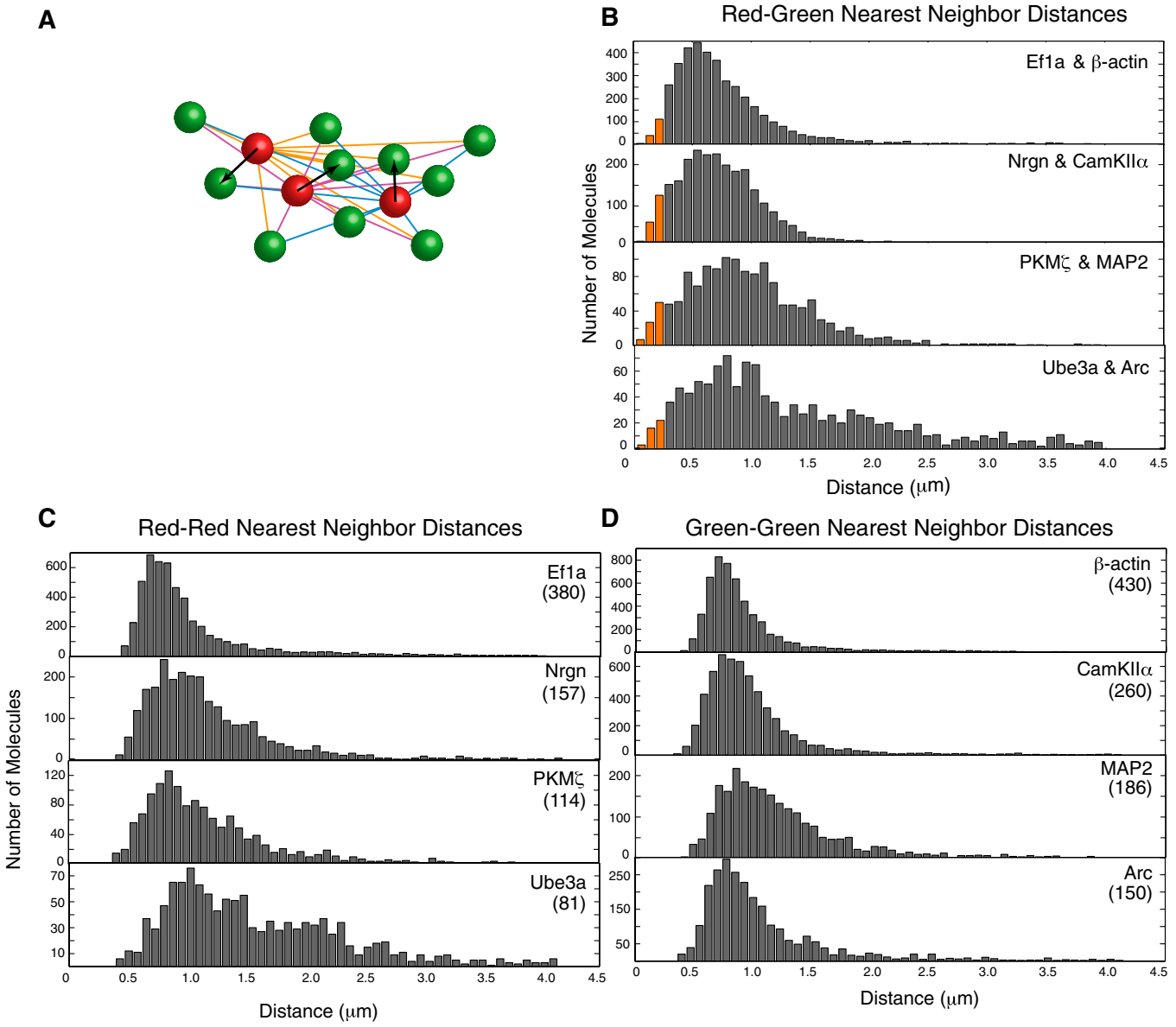

Fig. S3. Distribution of nearest neighbor distances between spots produced by pairwise combinations of different mRNA species in hippocampal neurons. (*A*) A schematic showing the measurements. The distances from each of the spots of the least-abundant mRNA species (red spots) to all of the spots produced by the other species (green spots) were measured, and the distances to the closest spots (nearest-neighbor distances identified by black arrows) were used in the plot in *B*. (*B*) Distributions of the nearest-neighbor distances of four representative pairwise combinations of mRNA species. The bars highlighted in orange correspond to RNAs that are considered to be colocalized using the 250-nm distance limit and are equivalent to the percentages reported in Table 1. (*C*) Nearest-neighbor distances for the less-abundant species among the pairs reported in *B*. (*D*) Nearest-neighbor distances for the more-abundant species among the pairs reported in *B*. The density of each mRNA is indicated as the number of mRNA molecules per neuron. Longer-tailed distributions in the sparsely populated mRNAs signify that the distributions relate to the mRNA density rather than to any specific tendency of clustering.

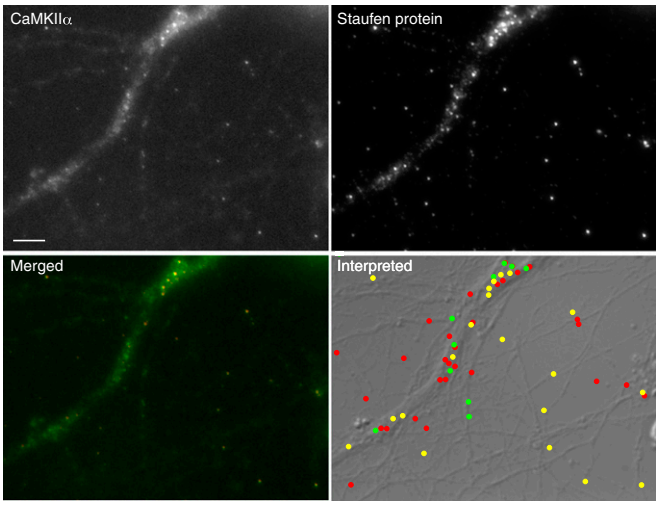

Fig. S4. CaMKIIα mRNA is present in granules that contain Staufen 1 protein. CaMKIIα mRNA was imaged by in situ hybridization using a set of 48 probes specific for it, and Staufen 1, a protein component of CaMKIIα-RNA granules, was imaged by immunofluorescence using an antibody specific for it. Because both protein and RNA gave spot-like signals, the same type of colocalization analysis could be carried out on the resulting spots as was carried out on pairs of mRNAs. The green color in the merged image on the lower left represents CaMKIIα mRNA, and the red color represents Staufen 1. The identity of the spots in the interpreted overlay is as follows: green, CaMKIIα mRNA; red, Staufen 1 protein; and yellow, colocalized CaMKIIα mRNA and Staufen 1 protein. (Scale bar, 5 μm.)

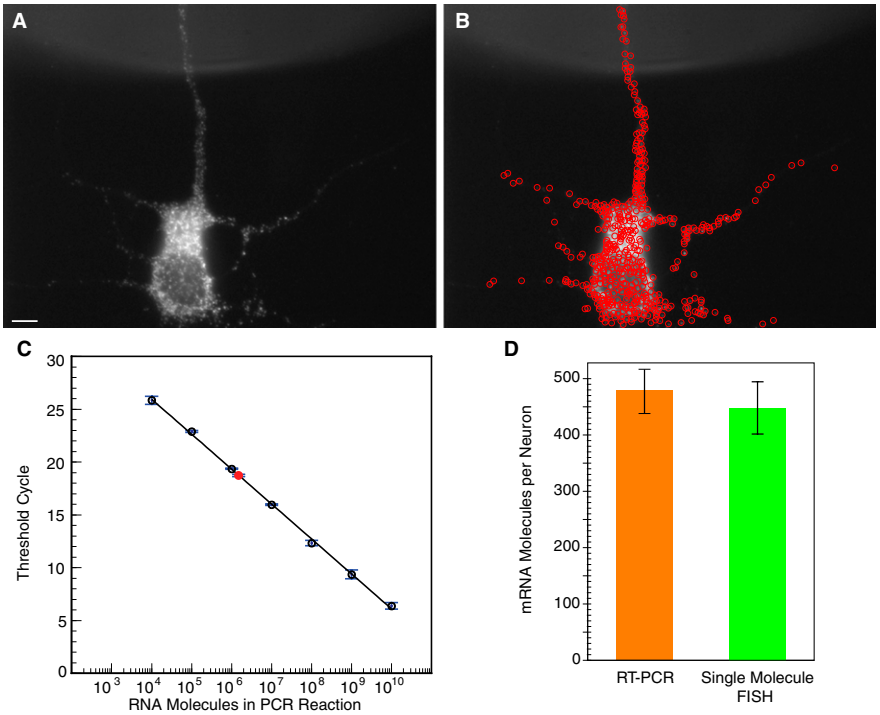

Fig. S5. Comparing the number of molecules of β-actin mRNA per neuron obtained by counting spots in the FISH images to the numbers obtained by real-time PCR performed on RNA extracted from the neurons. (*A*) Merged *z*-stacks of neurons imaged after hybridizing with probes for β-actin mRNA. (*B*) Identified spots are overlaid onto the image shown in *A* to demonstrate that almost all β-actin mRNA molecules are counted by our algorithm. (*C*) Quantification of mRNA copy number by real-time RT-PCR. A standard curve obtained from serial dilutions of full-length in vitro-transcribed β-actin RNA is shown. The red dot identifies the result obtained from reactions initiated by RNA isolated from resting neurons. (*D*) Comparison of the mRNA molecules per neuron determined by single-molecule FISH to the mRNA copy number per neuron determined by real-time PCR. The error bars represent 95% confidence intervals (in the case of PCR, the uncertainty in the measurement is dominated by uncertainty in cell counting, rather than uncertainty in PCR). (Scale bar, 5 μm.)

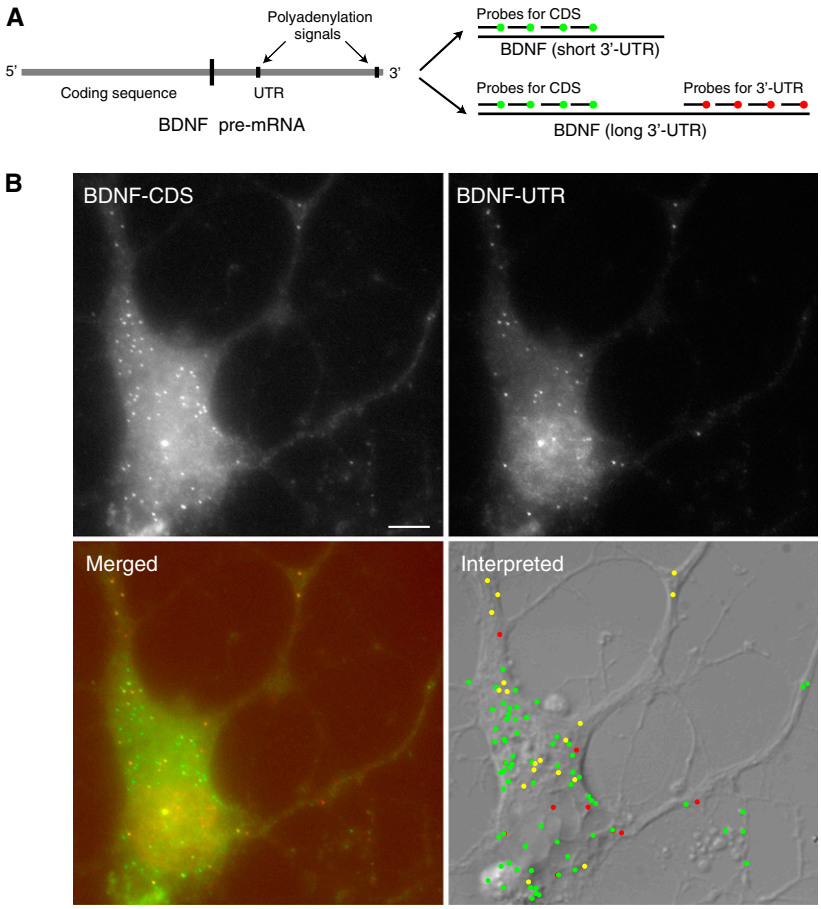

Fig. S6. Imaging two isoforms of BDNF mRNA with two sets of differently colored probes. (*A*) Due to the alternative utilization of two different polyadenylation sites, BDNF mRNA is found in two isoforms: a short isoform that uses a polyadenylation signal proximal to the coding sequence and a longer isoform that uses a relatively distal polyadenylation signal (UTR). The locations of the binding sites for the two differently colored sets of probes that were used to visualize these isoforms are indicated in the schematic diagram. (*B*) The two probe sets were used simultaneously to image BDNF mRNA isoforms. (*Upper* panels) Merged *z*-sections for the two differently colored probe sets. (*Lower Left*) Obtained by coding the spots from the coding sequence-specific probe set green and the spots from the UTR-specific probe set red. (*Lower Right*) An interpreted overlay in which colocalized spots from the two sets of probes (representing the long isoforms) are shown as solid yellow circles; spots labeled only by the coding sequence-specific probe set (representing the short isoforms) are shown as solid green circles; and spots labeled only by the UTR-specific probe set (that likely result from partial degradation of the long BDNF mRNA isoforms) are shown as solid red circles. Seventeen percent of the molecules were long isoforms. In addition to providing a measure of the distribution of the two isoforms, these images provide further support for the single-molecule sensitivity of the method because, if the spots arose from clusters of many mRNA molecules, we would not have observed the two isoforms in separate spots. (Scale bar, 5 μm.)

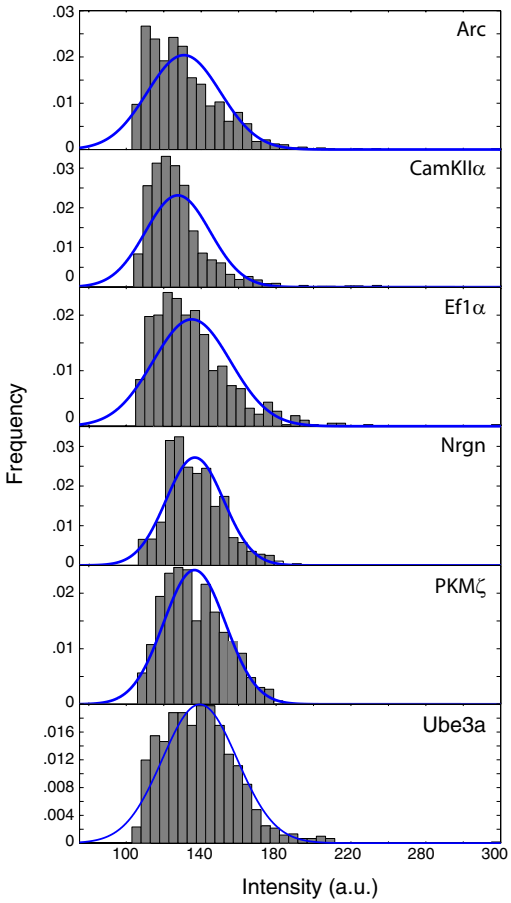

Fig. S7. Distribution of the intensities of spots produced by the hybridization of probe sets specific for different dendritic mRNAs. The blue curves are unimodal Gaussian fits overlaid on the histograms.

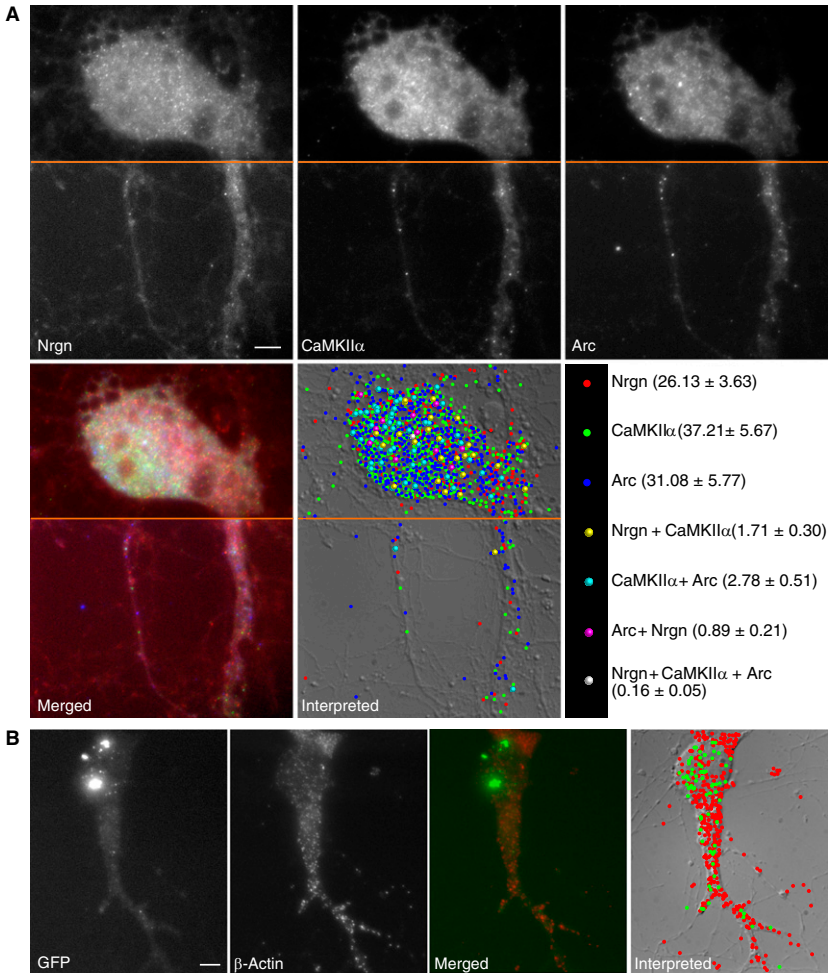

Fig. S8. mRNAs with the same dendritic localization elements show little or no tendency to colocalize with each other. (*A*) Triplex imaging of three mRNAs. Merged *z*-sections of a representative neuron, where each panel is an image of the cell seen in the fluorescence channel that detects one of the three differently colored probe sets used to distinguish these mRNA species (*Upper*). These images were merged into a single colored image of the cell (*Lower Left*) and were analyzed to identify solitary and colocalized spots. The resulting locations of all spots are indicated on a DIC image of the cell (*Lower Right*), in which the locations of the mRNA molecules are indicated by solid circles whose color identifies whether they are inferred to be solitary or colocalized (see the key on the right). The key also includes the average percentage of different kinds of solitary and colocalized molecules that were seen in 20 neurons with a 95% confidence interval. The horizontal orange line on each image separates the soma from the dendrites. (*B*) An engineered mRNA that contains both a GFP-coding sequence and the DTE from the 3′-UTR of β-actin mRNA does not colocalize with endogenous β-actin mRNA (which contains the same DTE). Neurons were infected with a lentivirus vector expressing this engineered mRNA, and their mRNAs were then hybridized in situ to a probe set specific for β-actin mRNA and to a differently colored probe set specific for GFP mRNA. The resulting image indicates that engineered mRNAs (green) migrated to the dendrites, but they were not colocalized with native β-actin mRNAs (red). (Scale bar, 5 μm.)

Table S1. Percent colocalization of total mRNA in soma (upper numbers) and dendrites (lower numbers)

	Arc	MAP2	CaMKIIα	Nrgn	PKMζ	Ube3a	Ef1α
β-Actin	2.61 ± 0.52	2.49 ± 0.36	1.81 ± 0.73	3.15 ± 0.76	1.49 ± 0.50	2.83 ± 0.62	1.99 ± 0.62
	0.43 ± 0.65	1.69 ± 0.63	0.71 ± 0.50	0.82 ± 0.81	0.45 ± 0.28	0.82 ± 0.41	0.81 ± 0.38
Arc		2.36 ± 0.94	3.80 ± 1.02	0.52 ± 0.33	1.30 ± 0.54	0.80 ± 0.55	3.08 ± 1.54
		1.17 ± 0.81	1.51 ± 1.40	0.06 ± 0.11	0.25 ± 0.26	0.25 ± 0.37	1.01 ± 0.58
MAP2			3.95 ± 0.75	3.51 ± 0.84	2.20 ± 0.65	3.84 ± 1.17	2.08 ± 0.37
			0.88 ± 0.55	3.19 ± 0.66	0.78 ± 0.58	2.57 ± 1.20	1.28 ± 0.51
CaMKIIα				2.00 ± 0.57	2.06 ± 0.70	2.21 ± 0.70	2.80 ± 0.92
				1.19 ± 0.64	0.69 ± 0.48	0.65 ± 0.45	2.10 ± 1.06
Nrgn					2.84 ± 0.54	0.42 ± 0.33	0.72 ± 0.22
					0.88 ± 0.65	0.15 ± 0.22	0.26 ± 0.19
PKMζ						2.85 ± 1.17	1.72 ± 0.63
						1.14 ± 1.50	0.49 ± 0.37
Ube3a							0.90 ± 0.34
							0.14 ± 0.17

Percentage of colocalization was calculated by dividing the number of molecules of mRNA species that were colocalized with the other mRNA species by the total number of mRNA molecules (within a ±95% confidence interval, where at least 10 neurons were examined).

Table S2. Percent colocalization of lower abundance mRNA in soma (upper numbers) and dendrites (lower numbers)

	Arc	MAP2	CaMKIIα	Nrgn	PKMζ	Ube3a	Ef1α
β-Actin	9.62 ± 1.79	8.10 ± 1.02	4.25 ± 1.63	14.5 ± 3.11	7.97 ± 2.99	12.4 ± 3.77	4.62 ± 1.28
	7.25 ± 9.03	5.50 ± 2.08	4.11 ± 2.52	5.74 ± 5.26	8.01 ± 6.80	2.73 ± 4.02	1.49 ± 0.83
Arc		5.39 ± 2.22	10.0 ± 3.09	1.77 ± 0.99	2.94 ± 1.48	2.59 ± 1.48	8.52 ± 2.27
		3.79 ± 3.71	4.52 ± 3.29	0.28 ± 0.28	0.65 ± 0.26	0.32 ± 0.46	6.03 ± 3.13
MAP2			7.16 ± 1.75	15.7 ± 6.14	5.87 ± 1.73	14.6 ± 4.87	9.10 ± 1.73
			6.24 ± 6.77	6.49 ± 2.34	2.03 ± 1.92	12.9 ± 8.70	4.66 ± 1.66
CaMKIIα				7.28 ± 1.21	8.60 ± 3.25	11.1 ± 3.07	8.42 ± 3.58
				3.41 ± 1.76	1.94 ± 1.43	2.52 ± 1.84	5.71 ± 1.57
Nrgn					8.10 ± 2.73	0.74 ± 0.57	2.67 ± 1.08
					1.69 ± 1.39	0.51 ± 0.85	0.90 ± 0.82
PKMζ						8.18 ± 3.40	10.5 ± 2.76
						5.70 ± 7.32	2.13 ± 2.24
Ube3a							5.31 ± 1.65
							1.57 ± 1.84

Percentage of colocalization was calculated by dividing the number of molecules of mRNA species that were colocalized with the other mRNA species by the number of lower abundance mRNA molecules (within a ±95% confidence interval, where at least 10 neurons were examined).

Other Supporting Information Files

Dataset S1 (XLS)